Drag Estimation in the Near Wake of the NREL's Airfoils Based on Hot-Wire Data

Vitalii Yanovych[1,2,*], *Daniel* Duda[1], *Václav* Uruba[1,2], and *Pavel* Antoš[2]

[1]University of West Bohemia, Univerzitní 8, 301 00 Pilsen, Czech Republic
[2]Institute of Thermomechanics of the Czech Academy of Sciences, Dolejškova 5, 182 00 Prague, Czech Republic

Abstract. This paper presents the results of the drag coefficient estimations for different types of NREL airfoils based on the experimental data. Namely, it was S803, S807, S813, and S817 profiles with the same chord length. The investigations were conducted at three angles of attack α=0°, α=±5°, different chord-based Reynolds numbers 0.6×10^5, 1.3×10^5 and 2.6×10^5. While, measuring cross-sections were placed behind the trailing edge at $x\cdot c^{-1}\approx$0.2, 0.4 and 1.0. Experimental data were collected using a hot-wire split fiber probe 55R55, which allowed us to estimate the characteristics of turbulent flow in stream-wise and crosswise directions. According to the obtained results, the highest and lowest *Cd* values correspond to profiles S817 and S803, respectively. Moreover, the results show that more asymmetric profiles S803 and S807 have the lowest resistance at zero angles of attack.

Research background: Application of Antonia and Rajagopalan methodology to drag assessment of various stream bodies.
Purpose of the article: Comparative evaluation of the drag coefficients of the NREL airfoils based on instantaneous velocity distribution behind.
Methods: Hot-wire anemometry with split fiber probe 55R55.
Findings & Value added: The highest drag coefficient corresponds to the S817 profile. The asymmetry of the airfoil shape has a significant impact on its drag characteristics.

Keywords: *Hot-wire, NREL's airfoils, wake topology, drag coefficient*

1 Introduction

Nowadays, investigations of the aerodynamic characteristics of the different airfoil types at relatively low chord-based Reynolds numbers less than 5×10^5 are becoming more actual from both fundamental and industrial points of view [1]. That is primarily due to the active development of innovations for small wind turbines [2], various types of drones, quadcopters, modern micro-air vehicles, and even biomechanics systems [3]. Despite their significance, the experimental data for lift and drag coefficients for low Re_c are only available for some airfoils. Usually, various aerodynamic scales are applied to determine these parameters, while

*Corresponding author: yanovych@kke.zcu.cz

for their prediction, using numerical simulations. Besides, the methodology proposed by Antonia and Rajagopalan has also become widely available to assess the drag forces of various streamlined bodies [4]. According to it, the aerodynamic forces can to determined using instantaneous velocity and its derivatives [5]. It allows obtaining drag data without surface instrumentation or external balance mechanism, which is particularly useful for different experimental techniques [6-9].

This paper aims to study by Hot-wire the behavior of the drag coefficient for different types of NREL's airfoils under various experimental conditions. These profiles family have become widespread in various fields because their geometry provides well lift-to-drag ratios. [10].

2 Experimental setup

The experiments were conducted at the Department of Power Engineering of the University of West Bohemia in the low-speed open-type wind tunnel, which has a test section 0.75 m long, 0.3 m high, and 0.2 m wide [11]. The natural level of turbulent inlet flow did not exceed 0.2 %.

Four types of NREL airfoil S803, S807, S813, and S817, were selected for the current study. They were produced of polymerized lactic acid (PLA) by 3D printing technology using the PRUSA i3 printer. In the general case, at 3D printing, the manufactured models are characterized by high surface roughness Ra ≈ 21.8 μm [12, 13]. Therefore, with the help of P2500 sandpaper with low abrasiveness, we have reduced the roughness to Ra ≈ 3~5 μm. The quality of roughness was estimated using a Taylor Hobson Surtronic Duo profilometer. All airfoil models have the same chord length and span of $c \approx 100$ mm and of $l \cdot c^{-1} \approx 1$, respectively. But at these dimensions, their thickness was different, namely for S803 – $b \cdot c^{-1} \approx 0.12$, S807 – $b \cdot c^{-1} \approx 0.18$, S813 – $b \cdot c^{-1} \approx 0.16$, and S817 – $b \cdot c^{-1} \approx 0.16$ (see Fig. 1 c).

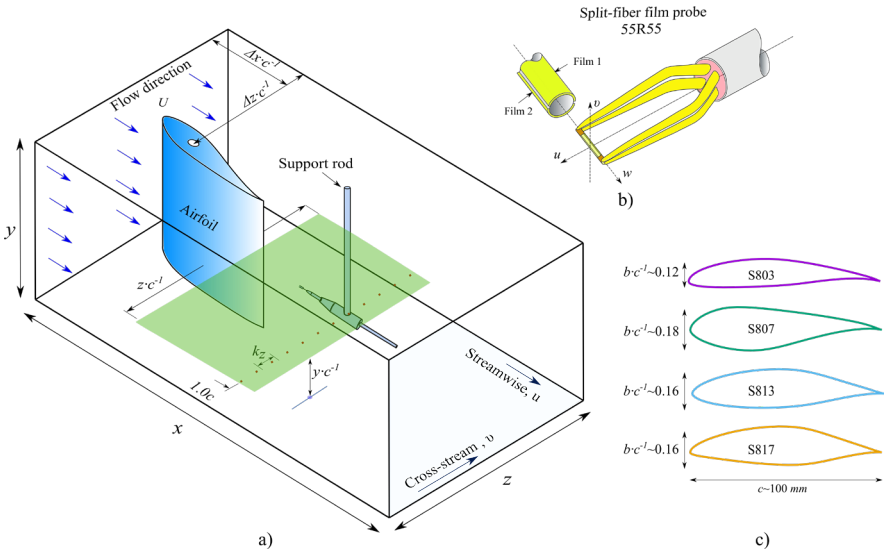

Fig. 1. a) The geometry configuration of the studied NREL airfoils. b) Sketches of the experimental setup. c) 55R55 split-fiber film probe. The arrows in blue indicate the direction of free-stream flow *U*. The green field shows the Hot-wire measuring plane. Where *b* and *c* the thickness and chord length of the airfoils. While $z \cdot c^{-1}$, $x \cdot c^{-1}$ and $y \cdot c^{-1}$ the width, length and location height of the measuring fields, respectively. The red dots line is the position of the measuring cross-section and k_z is the distance between the measuring points. The coordinates $\Delta z \cdot c^{-1} \approx 1.9$ and $\Delta x \cdot c^{-1} \approx 2.8$ shows the position of the aerodynamic center of the airfoil.

Measurements were performed at three flow velocities $U \approx 10$, 20 and 40 $m \cdot s^{-1}$. Thus, the chord-based Reynolds number Re_c was around 0.6×10^5, 1.3×10^5 and 2.6×10^5. The angle of attack also had three positions, α=0° and α=±5°, that varied by a stepper motor. It should note that, accordingly to the airfoil geometry, at zero angles, the blockage ratio is equal to 2.1-2.3%, while for the positive and negative angles, it is about 3%. Respectively to the Pope and Harper, this value cannot exceed 7.5%. Otherwise, an appropriate blockage correction method must be applied to the experiments. Mainly, the wake topology was analyzed in the measuring cross-section from $z \cdot c^{-1} \approx -0.5$ to 0.5 at $x \cdot c^{-1} \approx 1.0$, and the height of $y \cdot c^{-1} \approx 1.8$. But for a qualitative assessment of wake evolution, some measurements were done at $x \cdot c^{-1} \approx 0.2$ and 0.4, also. The sketch of the airfoil model and its set-up in the test section presents in Fig. 1 a.

The 55R55 split-fiber film Hot-wire probe was applied to study the two-dimensional characteristics of turbulent flow behind airfoil (see Fig. 1 b). The general uncertainty of the measurements was approximately ± 0.5%. The Hot-wire signals for all experiments were sampled at 70 kHz. The filtering of the received signal was applied as well. For the high and low pass filter the frequency was 10 Hz, and 30 kHz respectively. The typical duration of a one-point measurement was 10 s.

3 Results and discussion

In current investigations, the average drag coefficient for each airfoil was estimated from the wake profiles of the mean velocity and Reynolds stresses, accordingly to the formula of Antonia and Rajagopalan [4]:

$$C_d = 2\int_{-\infty}^{\infty} \frac{u}{U} \cdot \left(1 - \frac{u}{U}\right) d\left(\frac{z}{c}\right) + 2\int_{-\infty}^{\infty} \left(\frac{\overline{v'^2} - \overline{u'^2}}{U^2}\right) d\left(\frac{z}{c}\right) \quad (1)$$

where u is the local mean velocity, U is the external velocity of undisturbed flow, $\overline{u'^2}$ and $\overline{v'^2}$ are the normal Reynolds stresses components in streamwise and cross-stream directions, while $z \cdot c^{-1}$ is a dimensionless coordinate of the measuring point in a cross-stream direction.

The above formula consists of two parts, where the first term reflects the momentum deficit and the second is the effect of turbulence fluctuation in stream-wise and crosswise directions. Generally, this dependence gives approximately constant values in the absence of backflows. That usually happens close to the bluff body due to the vortex formation behind it. One of the main issues in drag predicting by velocity profiles is at what distance from the aerodynamic profile we need to integrate to correctly evaluated the drag coefficient. Many papers are devoted to this point. For example, according to [14], if the integration operation is performed at a cross-section where the local velocity is less than $0.5U$, the resulting value of the momentum deficit will have significant inaccuracies causing a serious underestimate of the drag coefficient. Moreover, in the airfoil drag investigation, the angle of its attack also plays an important role. Because a larger angle leads to the increasing bluntness, thus promoting the intensity of vortices separation from the airfoil [15]. As a result, the integral value of the second part of equation 1, which is responsible for fluctuating forces, increases sharply.

First, using the 55R55 hot-wire probe, we estimated the patterns of the velocity deficit with increasing distance from the trailing edge of the studied airfoils. The normalized streamwise velocity distribution $u \cdot U^{-1}$ along the wake centerline at $Re_c \approx 0.6 \times 10^5$, depending on the incident angles α and the distance $x \cdot c^{-1}$ shown in Fig. 2.

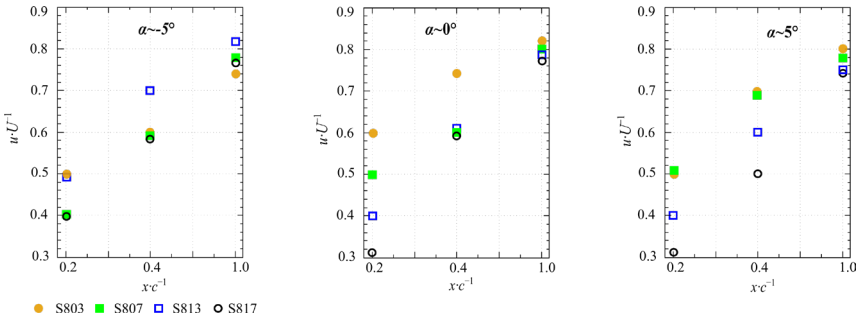

Fig. 2. Normalized streamwise velocity distribution $u \cdot U^{-1}$ along the wake centerline at $Re_c \approx 0.6 \times 10^5$, depending on the incident angles α and the distance $x \cdot c^{-1}$ behind airfoils.

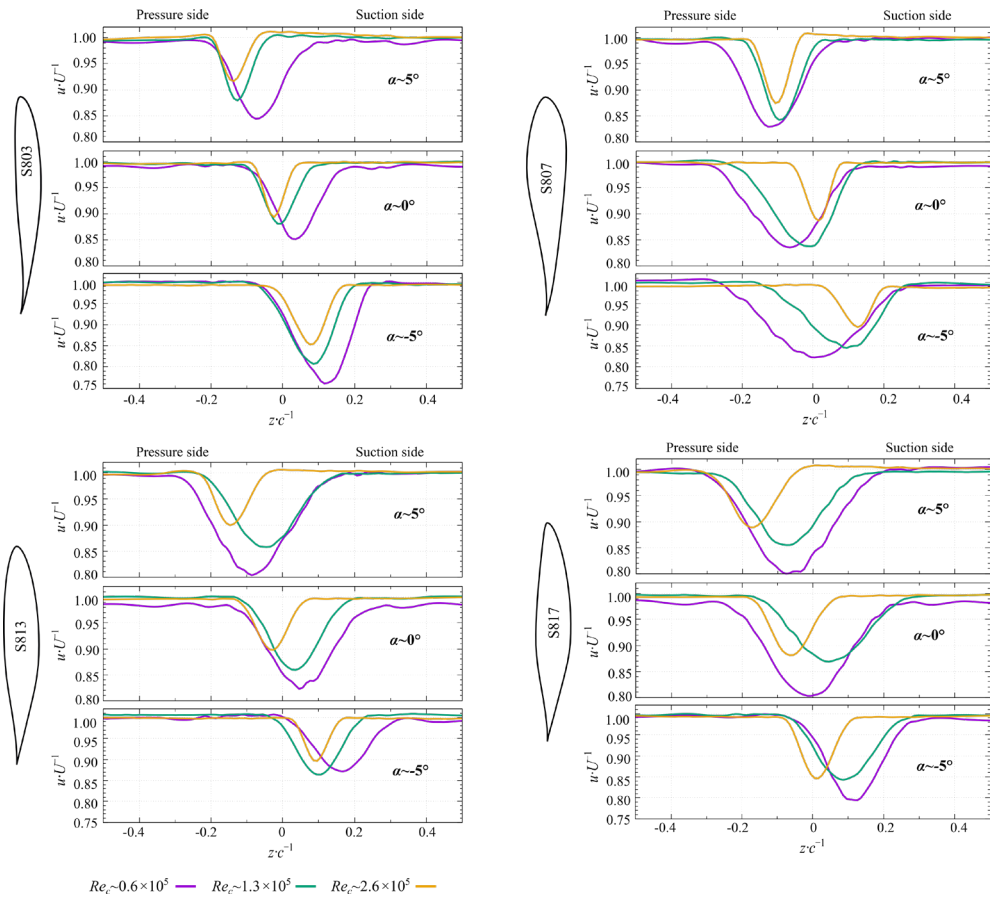

Fig. 3. Normalized streamwise velocity profiles $u \cdot U^{-1}$ at $x \cdot c^{-1} \approx 1.0$, depending on the airfoil types and incident angles α. Violet, green and yellow curves characterize the obtained data at $Re_c \approx 0.6 \times 10^5$, 1.3×10^5 and 2.6×10^5, respectively.

As we can see, with increasing distance up to $x \cdot c^{-1} \approx 1$, the velocity deficit decreased from 0.3−0.6 up to 0.8. Moreover, the last value of $u \cdot U^{-1}$ is approximately the same for all airfoil types, regardless of the angles of attack. Whereas, close to the trailing edge, the effect of profile geometry increases significantly. That is especially clear at $x \cdot c^{-1} \approx 0.2$ and $\alpha = 0°$,

where the velocity deficit for S817 is almost twice high as for S803. This result is somewhat unexpected, as the thickest among the studied airfoils is the S807 profile (see Fig. 1 c).

Based on the above data for further analysis, we chose the cross-section at $x \cdot c^{-1} \approx 1$. At this distance, we evaluated the distribution of the velocity characteristics behind different airfoil types (stream-wise component only), depending on the angle of attack and various Reynolds numbers (see Fig. 3). For better visualization, the obtained data were normalized to the average freestream velocity U and placed relative to the trailing edge of airfoils at α=0°. The received results permitted us to estimate the dimensions of the wake. In general, we can observe that as the Reynolds number increases, the depth and width of the wake decrease. Accordingly, to the airfoil thickness, the largest and smallest wake widths correspond to profiles S807 and S803, respectively. This feature is especially noticeable at α =−5°, where the wake at S807 are three times thicker than at S803.

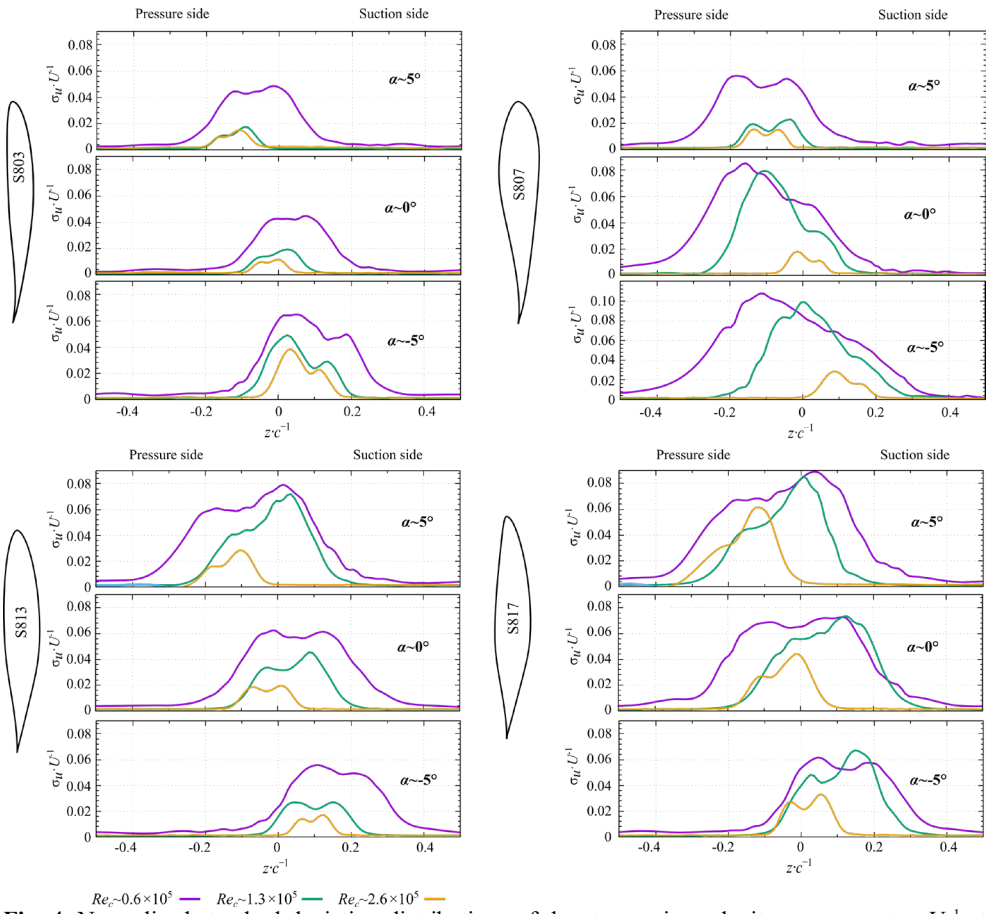

Fig. 4. Normalized standard deviation distributions of the streamwise velocity component $\sigma_u \cdot U^{-1}$ at $x \cdot c^{-1} \approx 1.0$, depending on the airfoil types and incident angles α. Violet, green and yellow curves characterize the obtained data at $Re_c \approx 0.6 \times 10^5$, 1.3×10^5 and 2.6×10^5, respectively.

We also evaluated the patterns of the normalized standard deviation distributions in the streamwise directions at $x \cdot c^{-1} \approx 1.0$ depending on the Reynolds number and angle of attack (Fig. 4). The obtained data showed that, the smallest value of $\sigma_u \cdot U^{-1}$ and the narrowest width of the perturbation area is inherent for the S803 at α=0°. Mainly this difference is due to the thinnest profile thickness. In general, the experimental results of the studied airfoils indicate

a sharp decrease in the value of $\sigma_u \cdot U^{-1}$ with increasing Reynolds number and the presence of double peaks of the data distributions. Usually, the double peak can be observed at a symmetrical airfoil and occurs due to the interaction of vortices between the pressure and suction sides. In our case, the appearance of this phenomenon may indicate a certain shape symmetry of the studied profiles. Thus, we can see that for S813 and S817 airfoil at α=0°, the double peak is more apparent. Whereas for the most asymmetric S807 profile, the obtained curve of $\sigma_u \cdot U^{-1}$ has only one pronounced peak from the pressure side.

It should note that another relative indicator of shape asymmetry may be the anisotropy of turbulent flow. What can be estimated using the Reynolds stress tensor [16]. Usually, it has six individual components that describe the flow characteristics relative to the three spatial directions. But in our case, the split fiber 55R55 probe provides measurements only in two directions. In this case, the Reynolds stress tensor becomes statistically two-dimensional. The normalized Reynolds shear stress distributions $\overline{u'v'} \cdot U^{-2}$ at $x \cdot c^{-1} \approx 1.0$, depending on the airfoil types and incident angles, are shown in Fig. 5.

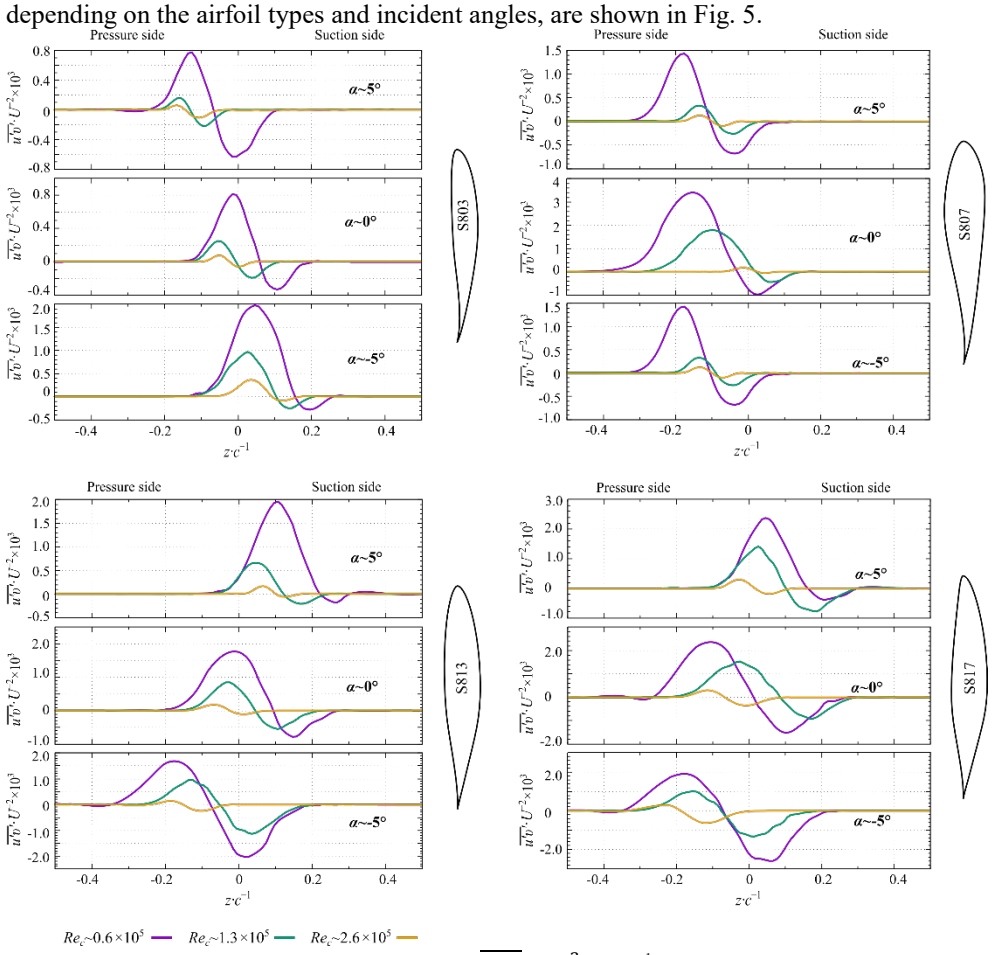

Fig. 5. Normalized Reynolds shear stress profiles $\overline{u'v'} \cdot U^{-2}$ at $x \cdot c^{-1} \approx 1.0$, depending on the airfoil types and incident angles α. Violet, green and yellow curves characterize the obtained data at $Re_c \approx 0.6 \times 10^5$, 1.3×10^5 and 2.6×10^5, respectively.

As we can see, the highest anisotropy is observed for S807 airfoil, while the lowest is for S803. Of course, such a pattern can be caused not only by the asymmetry of the geometry but also by the airfoil thickness.

Moreover, the characteristics of $\overline{u'v'} \cdot U^{-2}$ for the S803 strongly depends on the Reynolds number. For example, when Re_c increases four times, the maximum value of $\overline{u'v'} \cdot U^{-2}$ decreases approximately five times. Besides, the data obtained show that regardless of the airfoil type, the perturbation region of shear stress with a negative value is located directly on the suction side. This behavior is due to the growth of turbulence intensity, which increases the frictional resistance of the flow. Another interesting fact is that the greatest width of the perturbation zone corresponds to the S817 profile. That is especially noticeable at zero angle of attack. It should note that, unlike others, this airfoil type has a maximum width close to the trailing edge. Thus, this feature of the geometry can cause such a difference.

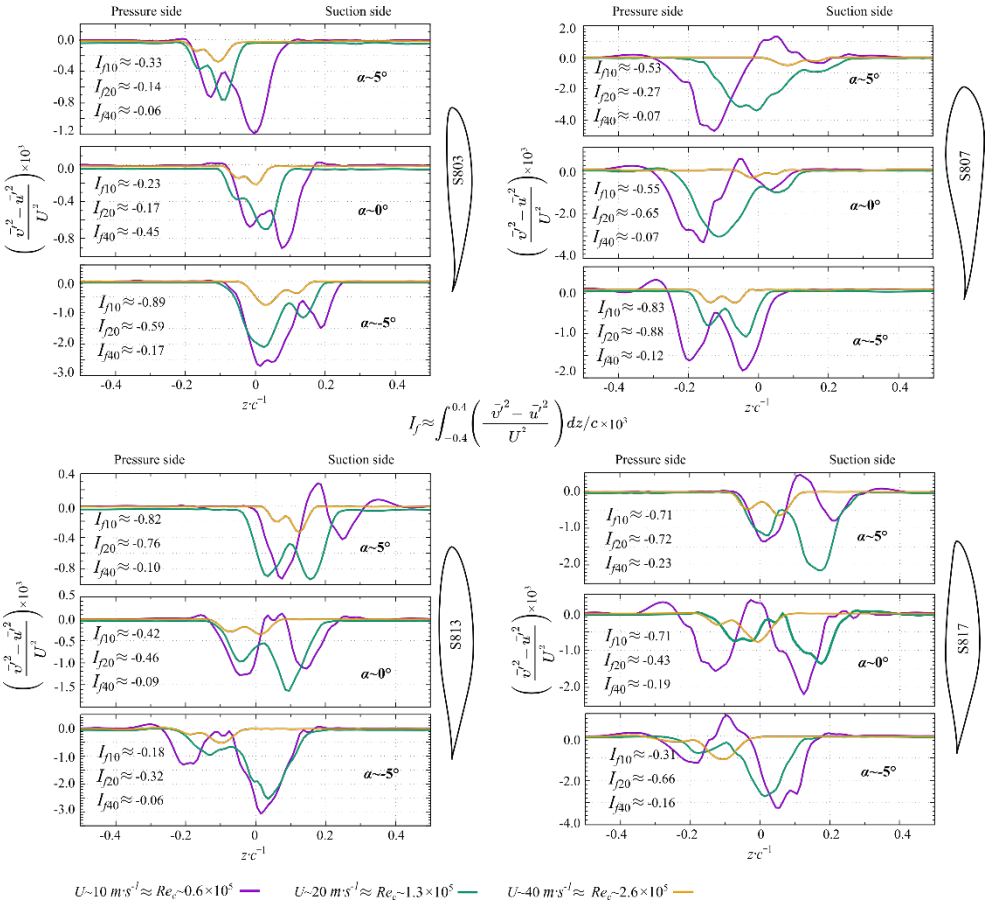

Fig. 6. Impact assessment of streamwise and cross-stream fluctuations on the drag coefficient (accordingly to Antonia and Rajagopalan [4]) for different airfoil types. Calculations were performed at $x \cdot c^{-1} \approx 1.0$ and at various incident angles α, where I_f is the integral value of the turbulence contribution for each measuring cases. Violet, green and yellow curves characterize the obtained data at $Re_c \approx 0.6 \times 10^5$, 1.3×10^5 and 2.6×10^5, respectively.

The next necessary part of our investigation was the analysis of the Reynolds normal stress components characteristics. Because exactly their difference forms the part of Antonia and Rajagopalan equation, which reflects the contribution of turbulent fluctuations on the drag coefficient. In Fig. 6 shows a graphical interpretation of the normalized difference between the cross-stream and streamwise velocity fluctuations at $x \cdot c^{-1} \approx 1.0$ depending on the

airfoil types, angle of attack, and different Reynolds numbers. Moreover, each graph also contains the integral value of the obtained distribution I_f for each measuring case. It should note that this parameter could be also interpreted as a complex indicator of the degree of flow anisotropy. Accordingly, to the obtained data, the value of I_f decreases with increasing Reynolds number from 0.6×10^5 to 2.6×10^5. Thus, at zero angles of attack, the magnitude of I_f reduces by: for S803−2 times, for S807−8 times, for S813−5 times, and for S817 is 4 times.

Finally, using the obtained data and equation (1), we calculated the characteristics of the drag coefficient *Cd* for each airfoil types depending on the incident angle and Reynolds numbers (see Fig. 7). The obtained data, regardless of the airfoil type, at flow velocity increasing shows logical drag growing. Moreover, the highest value of *Cd* is inherent for S817, while for S803, it is the lowest. That is a somewhat unexpected result, as the S807 is the thickest of the investigated airfoils (see Fig. 1 c). Besides, we can also observe the influence of airfoil shape asymmetry on the drag coefficient characteristics. Thus, for S803 and S807, its minimum value is detected at α=0°, whereas at α=±5°, *Cd* increases sharply. While the maximum drag values for S813 and S817 are observed at α=+5° and α=−5°, respectively.

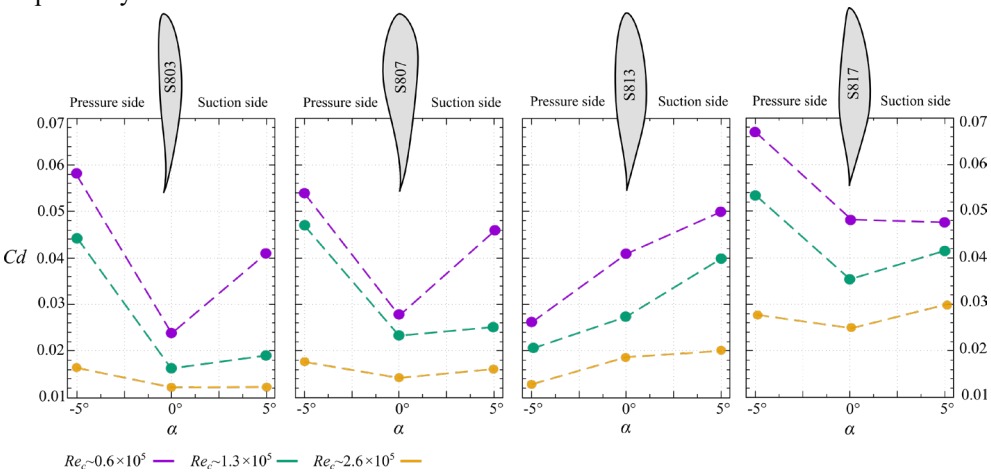

Fig. 7. Distribution of the drag coefficient *Cd* for different airfoil types depending on the incident angle and Reynolds numbers. Violet, green and yellow curves characterize the obtained data for $Re_c \approx 0.6\times10^5$, 1.3×10^5 and 2.6×10^5, respectively.

4 Conclusion

The drag coefficient in the near wake of the different NREL's airfoils was estimated. Namely, it was the profiles S803, S807, S813, and S817. Hot-wire anemometry with a split-fiber film probe 55R55 was applied to the data collection. Experimental investigations realized in several measuring cross-sections, at different Reynolds numbers 0.6×10^5, 1.3×10^5, 2.6×10^5, three angles of attack α= ±5°and 0°. As a result of the study, we obtained a series of graphical distributions for velocity characteristics, standard deviation, and Reynolds stress components. That allowed us to assess the wake topology for each measuring case. Then, using the methodology of Antonia and Rajagopalan, we evaluated the values of the drag coefficients for different airfoil types. Comparative analysis of the data showed that the highest and lowest value of *Cd* corresponds to S817 and S803 profiles, respectively. Moreover, the obtained results displayed that for S803 and S807 profiles, the minimum drag coefficient manifests at α=0°. Whereas for S813 and S817, it was detected at negative and positive angles of attack, respectively.

This work was supported by the project "Research and development of power machines and equipment" reg. No. SGS-2022-023.

References

1. Zhou, M d. Mahbub Alam, Yang, H.X., Guo, H., Wood, D.H. (2011). Fluid forces on a very low Reynolds number airfoil and their prediction. *International Journal of Heat and Fluid Flow*, 32(1), 329-339.
2. Brendel, M., Mueller, T.J. (1988). Boundary-layer measurements on an airfoil at low Reynolds number. *Aircraft*, 25, 317-612.
3. Usherhood, J.R., Ellington, C.P. (2002). The aerodynamics of revolving wings, I. Model hawkmoth wings. *Journal of Experimental Biology*, 205(11), 1547-1564.
4. Antonia, R.A., Rajagopalan, S. (1990). Determination of drag of a circular cylinder. *AIAA Journal*, 28(10), 1833-1834.
5. Son, O., Cetiner, O. (2016). Drag Prediction in the Near Wake of a Circular Cylinder based on DPIV Data. *Journal of Applied Fluid Mechanics*, 9, 1963-1968.
6. Brennan, J.C., Fairhurst, D.J., Morris R.H., McHale, G., Newton, M.I. (2014). Investigation of the drag reducing effect of hydrophobized sand on cylinders. J*ournal of Physics D: Applied Physics*, 47(20), 205302.
7. Cao, S., Ozono, S., Tamura, Y., Ge, Y., Kikugawa, H. (2010). Numerical simulation of Reynolds number effects on velocity shear flow around a circular cylinder. *Journal of Fluids and Structures*, 26(5), 685-702.
8. Goodfellow, S.D., Yarusevych, S., Sullivan, P.E. (2012). Momentum coefficient as a parameter for aerodynamic flow control with synthetic jets. *AIAA Journal*, 51(3), 623-631.
9. Henderson, R.D. (1995). Details of the drag curve near the onset of vortex shedding. *Physics of Fluids*, 7(9), 2102-2104.
10. Tangler, J. Somers, D. (1995). *NREL airfoil families for HAWT's*, report of the National Renewable Energy Laboratory (January 1995, Cole Boulevard Golden, Colorado, USA).
11. Yanovych, V., Duda, D., Uruba, V. (2021). Structure turbulent flow behind a square cylinder with an angle of incidence. *European Journal of Mechanics, B/Fluids*, 85, 110-123.
12. Yanovych, V., Duda, D., Uruba, V., Tomášková, T. (2022). Hot-Wire Investigation of Turbulence Topology behind Blades at Different Shape Qualities. *Processes*, 10(3), 522.
13. Yanovych, V., Duda, D., Horáček, V., Uruba, V. (2019). *Research of a wind tunnel parameters by means of cross-section analysis of air flow profiles. AIP Conference Proceedings*, 2189, 020024.
14. Son, O., Cetiner, O. (2016). Drag Prediction in the Near Wake of a Circular Cylinder based on DPIV Data. *Journal of Applied Fluid Mechanics*, 9, 1963-1968.
15. Duda, D., Uruba, V., Yanovych, V. (2021). Wake width: Discussion of several methods how to estimate it by using measured experimental data. *Energies*, 14(15), 4712.
16. Yanovych, V., Duda, D., Uruba, V., Antoš, P. (2021). Anisotropy of turbulent flow behind an asymmetric airfoil. *SN Applied Sciences*, 3(12), 885.